Fortschritte der Physik

Fortschritte der Physik
Progress of Physics
www.fp-journal.org

RESEARCH ARTICLE OPEN ACCESS

Approximate Ricci-Flat Metrics for Calabi–Yau Manifolds

Seung-Joo Lee[1] | Andre Lukas[2]

[1]Department of Physics, Yonsei University, Seoul, Republic of Korea | [2]Rudolf Peierls Centre for Theoretical Physics, University of Oxford, Oxford, UK

Correspondence: Seung-Joo Lee (seungjoolee@yonsei.ac.kr)

Received: 13 March 2026 | **Revised:** 13 June 2026 | **Accepted:** 16 June 2026

Keywords: algebraic geometry | ansatz | differential geometry | mathematical analysis | mathematics | modulus | pure mathematics | string theory

ABSTRACT

We outline a method to determine analytic Kähler potentials with associated approximately Ricci-flat Kähler metrics on Calabi–Yau manifolds. Key ingredients are numerically calculating Ricci-flat Kähler potentials via machine learning techniques and fitting the numerical results to Donaldson's ansatz. We apply this method to the Dwork family of quintic hypersurfaces in $\mathbb{P}^4$ and an analogous one-parameter family of bi-cubic CY hypersurfaces in $\mathbb{P}^2 \times \mathbb{P}^2$. In each case, a relatively simple analytic expression is obtained for the approximately Ricci-flat Kähler potentials, including the explicit dependence on the complex structure parameter. We find that these Kähler potentials only depend on the modulus of the complex structure parameter.

1 | Introduction

Yau's theorem guarantees the existence of a unique Ricci-flat Kähler metric with a given Kähler class on a Calabi–Yau (CY) manifold. Such Ricci-flat metrics are of mathematical interest and they play an important role in compactifications of string theory. Unfortunately, for compact Calabi–Yau manifolds of complex dimension three or higher, analytic expressions for Ricci-flat metrics are not known. Over the past few years substantial progress has nevertheless been made in numerically computing Ricci-flat metrics on Calabi–Yau three-folds, starting with Donaldson's algorithm [1] and its applications [2–9] and, more recently, using machine learning methods [10–16].

The Ricci-flat metric in numerical form is already useful, enabling us to compute the spectrum of the Laplacian on a CY manifold [5, 17] or the masses of quarks in a CY string compactification [18], to name just two applications. However, it would be all the more helpful and exciting to deal with the metric analytically. The purpose of this paper is to present analytic expressions for metrics (or, rather, their associated Kähler potentials) on relatively simple CY manifolds, which are approximately Ricci-flat. More specifically, we will find such metrics for the standard one-parameter Dwork family of quintics, as well as an analogous one-parameter family for the bi-cubic CY. For these cases, we will obtain a family of approximately Ricci-flat analytic metrics as an explicit function of the single complex structure modulus.[1]

The starting point of our discussion is Donaldson's ansatz for CY metrics. Consider a CY manifold X, an ample line bundle $L \to X$ and a basis $\{s^I\}$ of sections of $\Gamma(X, L^k)$, where k is a positive integer. Then, Donaldson's ansatz for the Kähler potential K reads

$$K = \frac{1}{\pi k}\log(\kappa)\ , \qquad \kappa = H_{I\bar{J}} s^I \bar{s}^{\bar{J}}\ , \tag{1.1}$$

where H is a Hermitian matrix to be determined. The associated Kähler form and the metric are given by $J = i\partial\bar{\partial}K$ and $g_{\alpha\bar{\beta}} = \partial_\alpha \partial_{\bar{\beta}} K$, respectively. Donaldson's algorithm involves finding, for any fixed k, a "balanced" metric, using an iterative procedure. It can be shown that these balanced metrics converge to the Ricci-flat metric with Kähler class $[J]$ proportional to $c_1(L)$, as $k \to \infty$. Practical numerical calculations can only be carried out up to a finite k (as the dimension of $\Gamma(X, L^k)$ increases) and reasonable numerical approximations to the Ricci-flat metric by balanced metrics can be obtained for moderately large k, say $k \geq 6$ [3]. Here, we will not attempt to find the balanced metric but ask instead about the “optimal” metric for a given k, that is, the metric within the family (1.1), which is “closest” to the Ricci-flat one. As we will see, this already leads to fairly accurate results for relatively small k, specifically $k = 1, 2, 3$.

In practice, we proceed as follows. Our chosen CY manifolds, the one-parameter families of quintics and bi-cubics, have relatively large discrete symmetries G. Restrictions thus arise on the form of the Hermitian matrix H in the Kähler potential (1.1), which we first clarify. Next, we use machine learning techniques, specifically the cymetric package [14], to compute the Kähler potential of the Ricci-flat metric numerically, for many choices of the single complex structure parameter ψ. We then fit the ansatz (1.1) to each of these numerical Kähler potentials and thereby determine the remaining coefficients (after having imposed the symmetry constraints mentioned above) of H as a function of ψ. In this way, we obtain remarkably accurate fits even for $k = 2$ and a relatively simple Kähler potential of the form (1.1) with explicit ψ-dependence, leading to the associated analytic expression for an approximately Ricci-flat metric.

The plan of the paper is as follows. In the next section, we introduce our method in detail by illustrating it with the standard one-parameter Dwork family of quintics. In Section 3, we consider a somewhat more complicated example, a one-parameter family of bi-cubic CY manifolds. We conclude in Section 4.

2 | Approximate Ricci-Flat Metrics on the Quintic

Our strategy starts from choosing a one-parameter family of quintics X with a symmetry group G and restricting the Kähler potential ansatz (1.1) by imposing G-invariance. This will reduce the number of free parameters in the Ansatz considerably and simplify the numerical calculation.

In fact, the procedure here is not quite as innocent as it might seem, because G may in general have fixed points. If G is freely acting, the quotient X/G is a smooth CY manifold with a unique Ricci-flat metric of its own, which, pulled back, gives rise to a Ricci-flat metric on X. In this case, the associated Ricci-flat Kähler potential should thus be G-invariant by construction. In the presence of fixed points, however, the above argument does not apply as simply due to the singularities of the quotient.

For the family of CY manifolds that we consider in this section (and also for the one considered in the following section), the symmetry G does lead to fixed points. Nevertheless, we can use a different argument to show that our non-freely acting symmetry must still be respected by the Ricci-flat metric: First, as it turns out, our symmetry G acts trivially on the Kähler class $[J]$ of a Ricci-flat Kähler form J. Then, for each $g \in G$, since the pull-back g^*J is also Ricci-flat and has the Kähler class $[g^*J] = g^*[J] = [J]$, the uniqueness of the Ricci-flat metric for a given Kähler class assures that $g^*J = J$, which is the required symmetry property.

For the explicit computation, we first obtain approximately Ricci-flat metrics (and the associated Kähler potentials) numerically, for many values of the complex structure parameter ψ, using the cymetric package. The results for any given ψ are then fit to the Kähler potential Ansatz (1.1) (in its G-invariant form). Combining the results for all values of ψ, we finally determine the ψ-dependence of the Kähler potential.

2.1 | Quintic Threefolds

We begin by introducing the properties of quintic CY threefolds, relevant to our discussion; see, for example, Ref. [20] for more information on the quintic, as well as other related Calabi–Yau manifolds, and Ref. [21] for mathematical background on manifolds with special holonomy. Quintic CY threefolds X have non-trivial Hodge numbers $(h^{1,1}(X), h^{2,1}(X)) = (1, 101)$ and Euler number $\eta(X) = -200$. They can be defined by the vanishing locus of a quintic polynomial in complex projective space $\mathbb{P}^4$, on which we introduce homogeneous coordinates x_A with $A = 0, \ldots, 4$. On a local patch, for example, the one defined by $x_0 \neq 0$, we have affine coordinates x_a/x_0 with $a = 1, \ldots, 4$. For our purposes, we consider the one-parameter Dwork family of quintics, whose defining polynomials are given by

$$P = x_0^5 + x_1^5 + x_2^5 + x_3^5 + x_4^5 - 5\psi\, x_0x_1x_2x_3x_4\,, \tag{2.1}$$

where $\psi \in \mathbb{C}$ is the single complex structure parameter (out of a total of $h^{2,1}(X) = 101$).

Note that we may impose the following identification on the complex structure:

$$\psi \sim \alpha\psi\,, \quad \text{for } \alpha = \exp(2\pi i/5)\,, \tag{2.2}$$

since the coordinate transformation $x_0 \mapsto \alpha x_0$, $x_a \mapsto x_a$ for $a = 1, \ldots, 4$, combined with $\psi \mapsto \alpha^{-1}\psi$, leaves the polynomial (2.1) invariant. In practice, this means we can restrict our calculation to the fundamental domain $0 \le \arg(\psi) < 2\pi/5$. Within this domain the quintic (2.1) defines a smooth manifold, except at the conifold point $\psi = 1$.

The above family of quintics has the well-known freely acting $\mathbb{Z}_5^{(1)} \times \mathbb{Z}_5^{(2)}$ symmetry (projectively) generated by

$$\mathbb{Z}_5^{(1)} \;:\; x_A \mapsto \alpha^A x_A\,, \qquad \mathbb{Z}_5^{(2)} \;:\; x_A \mapsto x_{(A+1)\,\mathrm{mod}\,5}\,. \tag{2.3}$$

In fact, there is an even larger, non-freely acting symmetry group,

$$G = \langle \mathbb{Z}_5^{(1)}, S_5 \rangle\,, \tag{2.4}$$

where S_5 permutes the homogeneous coordinates x_A, which leaves the polynomials (2.1) invariant.

2.2 | Kähler Potential Ansatz

Choosing $L = \mathcal{O}_X(1)$ and starting with $k = 1$, we should consider the sections in $\Gamma(X, \mathcal{O}_X(1))$, a five-dimensional space spanned by the coordinates x_A, where $A = 0, \ldots, 4$. In this case, the ansatz (1.1) reads

$$K = \frac{1}{\pi} \ln\left(\sum_{A,\bar{B}=0}^{4} H_{A\bar{B}} x_A \bar{x}_{\bar{B}} \right), \tag{2.5}$$

where H is a Hermitian 5×5 matrix. For quintics defined by the polynomials (2.1), we expect K to respect the symmetry G, so we should consider only the G-singlets in $\Gamma(X, \mathcal{O}_X(1)) \times \Gamma(X, \mathcal{O}_X(1))^*$. There is evidently only one such singlet, which corresponds to a matrix H proportional to the unit matrix. After absorbing the factor of proportionality into a projective coordinate re-scaling the Kähler potential becomes

$$K = \frac{1}{\pi} \ln \left(\sum_{A=0}^{4} |x_A|^2 \right), \tag{2.6}$$

that is, the standard Fubini-Study Kähler potential.[2] No degree of freedom of the matrix H remains. This Fubini-Study Kähler potential (restricted to the quintic, using $P = 0$) represents a (rather crude) approximation to the Ricci-flat Kähler potential. Perhaps surprisingly, even this crude approximation leads to reasonable results for the purpose of some calculations [18].

To proceed more systematically, we incorporate the dependence of K on the complex structure parameter ψ as well as the Kähler parameter t, by using the $k = 1$ ansatz

$$K = c\, t \ln(\kappa) , \qquad \kappa = a_0 I_0 , \tag{2.7}$$

where I_0 denotes the G-singlet,

$$I_0 = \sum_{A=0}^{4} |x_A|^2 , \tag{2.8}$$

and the parameter $c \in \mathbb{R}$ accounts for the overall normalization. The single remaining degree of freedom of the matrix H, the parameter $a_0 = a_0(\psi)$, amounts to a Kähler transformation. As a result, the metric associated to Equation (2.7) is ψ-independent, as expected from the above arguments.

For a better approximation of the Ricci-flat metric, we proceed naturally to $k = 2$ and sections of $\Gamma(X, \mathcal{O}_X(2))$, a 15-dimensional space spanned by the quadratic monomials $x_A x_B$, where $A, B = 0, \ldots, 4$ and $A \leq B$. Again, we expect K to respect the symmetry G and focus on the G-singlets in $\Gamma(X, \mathcal{O}_X(2)) \times \Gamma(X, \mathcal{O}_X(2))^*$. As it turns out, there are precisely two such singlets, namely

$$I_0 = \sum_{A<B} |x_A|^2 |x_B|^2 , \qquad I_1 = \sum_{A} |x_A|^4 . \tag{2.9}$$

Therefore, the ansatz (1.1) for the Kähler potential can be written as

$$K = c\, t \ln(\kappa) , \qquad \kappa = a_0 I_0 + a_1 I_1 \tag{2.10}$$

where, again, t is the single Kähler parameter and $c \in \mathbb{R}$ a constant, while the two remaining degrees of freedom, $a_0 = a_0(\psi)$ and $a_1 = a_1(\psi)$ of the matrix H, are real functions of the complex structure parameter ψ. Our goal is to determine the functional forms of $a_0(\psi)$ and $a_1(\psi)$ by a comparison with numerical calculations.

Before we do so, let us also discuss the situation at the next higher order, $k = 3$. In this case, we should consider sections of $\Gamma(X, \mathcal{O}_X(3))$, a 35-dimensional space spanned by the cubic monomials $x_A x_B x_C$, where $A, B, C = 0, \ldots, 4$ and $A \leq B \leq C$. The space $\Gamma(X, \mathcal{O}_X(3)) \times \Gamma(X, \mathcal{O}_X(3))^*$ contains three G-invariants which are given by

$$I_0 = \sum_{A<B<C} |x_A|^2 |x_B|^2 |x_C|^2 , \qquad I_1 = \sum_{A \neq B} |x_A|^4 |x_B|^2 ,$$
$$I_2 = \sum_{A} |x_A|^6 . \tag{2.11}$$

This means that the ansatz for the Kahler potential is now of the form

$$K = c\, t \ln(\kappa) , \qquad \kappa = a_0 I_0 + a_1 I_1 + a_2 I_2 , \tag{2.12}$$

where, as before, the coefficients $a_r = a_r(\psi)$ with $r = 0, 1, 2$ are real functions of the complex structure parameter ψ.

2.3 | Numerical Results

We would like to consider quintics defined by Equation (2.1) for values of the complex structure parameter $\psi = 0.4\, n \exp(2\pi i m/25)$, where $n = 0, \ldots 50$ and $m = 0, \ldots 5$, leading to a total of 301 points and covering the fundamental domain[3] $0 \leq \arg(\psi) < 2\pi/5$ in the range $0 \leq |\psi| \leq 20$. The single Kähler parameter is set to $t = 1$; the Kähler potential and the metric scale with t, so the t-dependence can easily be restored later. For each of the above ψ-values, we use the cymetric point generator to generate a data set of 100000 points p_i on the manifold. We have checked that these data sets respect the G symmetry to good accuracy, that is, for each data point p the data set also contains points close to the orbit points Gp.

Using the cymetric ϕ-model we train a fully connected neural network (width 64, depth 3, GeLU activation) for each of the 301 data sets for 120 epochs. The final Monge–Ampere loss, as defined in Ref. [14], as a function of $|\psi|$ is shown in Figure 1 on the left. It is in the range 0.01–0.025, indicating that we have found Ricci-flat Kähler metrics to a good approximation. Using the trained networks, we read out the pairs (p_i, K_i), where K_i denote the values of the numerical Kähler potential evaluated at the points p_i. We may then use this Kähler potential data to determine the coefficients c and a_r in the ansätze (2.7), (2.10), and (2.12) as follows.

We begin with the somewhat trivial case $k = 1$, that is, the Fubini-Study metric (2.7). We have performed a fit to this ansatz for all 301 data sets, each consisting of 100000 pairs (p_i, K_i), to determine the optimal choices for the parameters c and a_0 in each case. The value of a_0 is not meaningful as it corresponds to a Kähler transformation and that of c is found to be approximately ψ-independent, $c \simeq 1/\pi$, in accordance with Equation (1.1). The mean of the relative deviation $|(K_i - K(p_i))/K(p_i)|$, evaluated from Equation (2.7) with the best-fit values for c and a_0 inserted, is shown in Figure 1 on the right (blue) for each $|\psi|$.

We move on to the case $k = 2$. As before, for all 301 data sets $\{(p_i, K_i)\}$ we have performed a fit to the Kähler potential ansatz (2.10), thereby determining the optimal parameters c and a_i in each case. The error for this ansatz with the best-fit values for the parameters, defined again as the mean of the relative deviation, is shown in Figure 1 on the right (yellow)

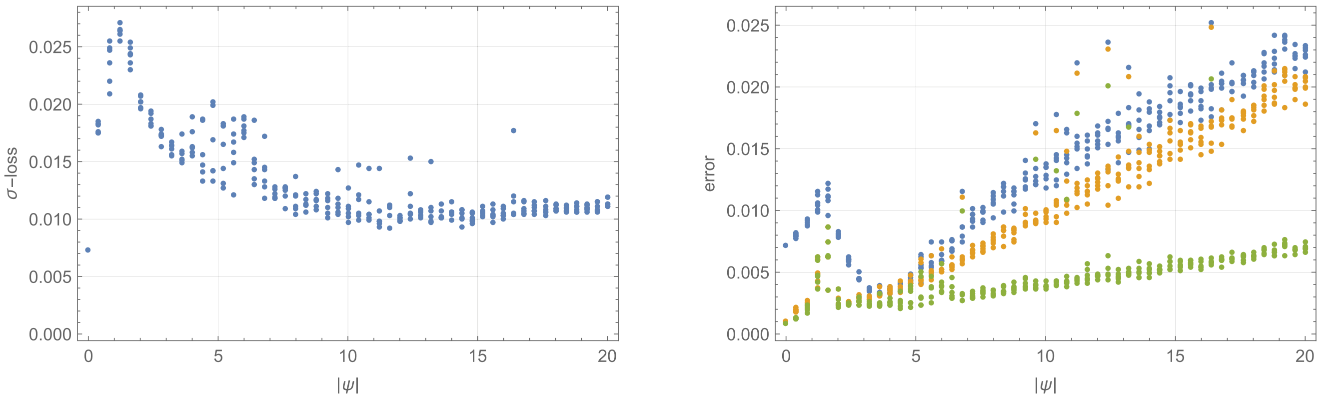

FIGURE 1 | Left plot: Final σ-loss as a function of $|\psi|$ for the quintic. Right plot: Mean of the relative error $|(K_i - K(p_i))/K(p_i)|$ as a function of $|\psi|$ for the Kähler $k = 1$ potential (2.7)(blue), the $k = 2$ Kähler potential (2.10) (yellow), and the $k = 3$ Kähler potential (2.12) (green).

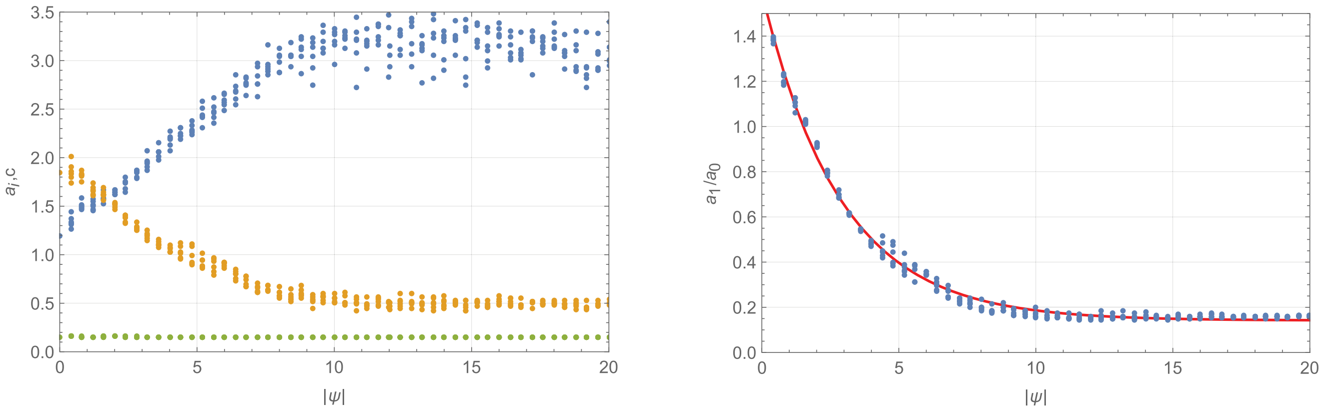

FIGURE 2 | Left plot: Best-fit coefficients $a_0(\psi)$ (blue) and $a_1(\psi)$ (orange) and c (green) in the Ansatz (2.10) for the quintic Kähler potential, as a function of $|\psi|$. Right plot: Ratio $a_1(\psi)/a_0(\psi)$ as a function of $|\psi|$ and best-fit of the form (2.14).

for each $|\psi|$. This error is about 2% at most for larger values of $|\psi|$ and somewhat smaller, around 1%, for small $|\psi|$-values. This means, Donaldson's ansatz for $k = 2$ can already provide an approximation to the Ricci-flat Kähler potential at the percent level, at least for our quintic example.

The optimal values for c and a_r as a function of $|\psi|$ for the $k = 2$ ansatz (2.10) are shown in Figure 2 on the left. The first observation from this figure is that the coefficient c is ψ-independent, as expected, and its value, $c \simeq \frac{1}{2\pi}$, is in good agreement with Equation (1.1). The other features in Figure 2 on the left look disappointing at first: the blue and the orange points which represent the optimal values of $a_0(\psi)$ and $a_1(\psi)$, respectively, have a rather substantial scatter, especially at larger values of $|\psi|$. There are two possible reasons why disappointment might be premature. First, there is no a priori reason why the a_i should be functions of the modulus $|\psi|$, rather than of the full complex variable ψ. Furthermore, the ambiguity of K due to Kähler transformations implies that $a_0(\psi)$ and $a_1(\psi)$ do not carry independent meaning; rather, the Kähler potential (2.10) can, equivalently, be written as

$$K = c\, t \ln\left(I_0 + \frac{a_1(\psi)}{a_0(\psi)} I_1\right) + \text{Kähler transformation}\,, \qquad (2.13)$$

which suggests plotting the ratio $\frac{a_1(\psi)}{a_0(\psi)}$ as opposed to the individual parameters $a_0(\psi)$ and $a_1(\psi)$. The resulting plot, as shown in Figure 2 on the right, strongly indicates that the ratio is a function of the modulus $|\psi|$ only. This function can, for example, be accurately fit by an exponential

$$f(|\psi|) = \frac{a_1}{a_0} \simeq 0.141 + 1.453\, e^{-0.348\,|\psi|}\,, \qquad (2.14)$$

whose graph is given by the red curve in Figure 2, on the right. This leads to the final form for the quintic Kähler potential,

$$K = \frac{t}{2\pi} \ln\left(I_0 + f(|\psi|) I_1\right). \qquad (2.15)$$

Here, I_0 and I_1 have been defined in Equation (2.9) and the ψ-dependence of K is fully encoded in the functional behavior of f, for which we can use Equation (2.14). This is a rather simple expression and the metric associated to this Kähler potential is approximately Ricci-flat to within a few percent.

Let us extend this discussion to the case $k = 3$, that is, to the Kähler potential ansatz (2.12), using the same data sets $\{(p_i, K_i)\}$ for complex structure parameters $\psi = 0.4\, n \exp(2\pi i m/25)$, where $n = 0, \ldots 50$ and $m = 0, \ldots 5$, as before. The best-fit values for c and

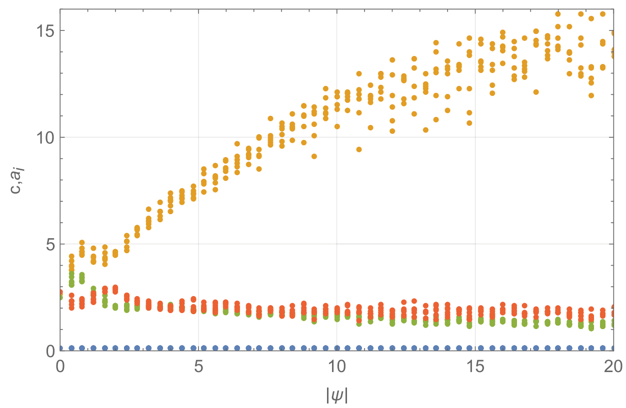

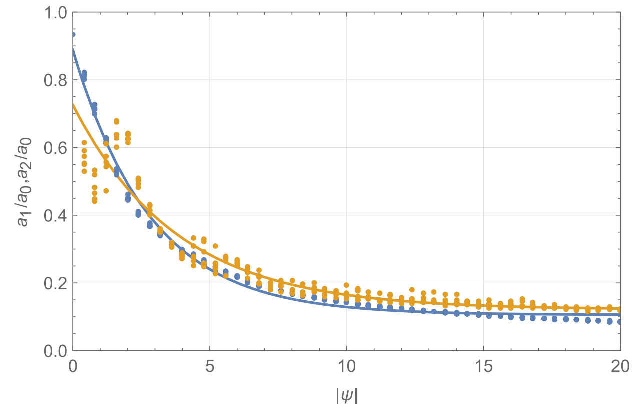

FIGURE 3 | Left plot: Best-fit coefficients $a_0(\psi)$ (yellow), $a_1(\psi)$ (red), $a_2(\psi)$ (green) and c (blue) in the Ansatz (2.12) for the quintic Kähler potential, as a function of $|\psi|$. Right plot: The ratios $a_1(\psi)/a_0(\psi)$ (yellow points) and $a_2(\psi)/a_0(\psi)$ (blue points) as a function of $|\psi|$ and best fits of the form (2.16).

$a_r(\psi)$ as a function of $|\psi|$ are shown in Figure 3. The mean error between the data and the ansatz (2.12) with these best-fit values inserted is shown in Figure 1 on the right (green). We note that this error is typically smaller than the one for $k = 2$ (yellow) and is below 1% for most ψ-values. In conclusion, the Ansatz (2.12) provides a rather good approximation to the Ricci-flat Kähler potential for the quintic.

From Figure 3 on the left, it is evident that the value of c is ψ-independent, as expected, and is given by $c \simeq \frac{1}{3\pi}$, in accordance with Equation (1.1). Furthermore, the scatter in Figure 3 on the left can be reduced significantly by considering the ratios $a_1(\psi)/a_0(\psi)$ and $a_2(\psi)/a_0(\psi)$, as Figure 3 on the right shows. This provides good evidence that a_1/a_0 and a_2/a_0 are functions of $|\psi|$ only and it turns out that the functional dependence is well described by the exponentials

$$f_1(|\psi|) = \frac{a_1}{a_0} \simeq 0.121 + 0.605\, e^{-0.264\,|\psi|} \,,$$
$$f_2(|\psi|) = \frac{a_2}{a_0} \simeq 0.106 + 0.783\, e^{-0.352\,|\psi|} \,, \tag{2.16}$$

whose graphs are shown in Figure 3, on the right. Hence, the final form of the approximately Ricci-flat Kähler potential for the quintic is given by

$$K = \frac{t}{2\pi} \log\left(I_0 + f_1(|\psi|) I_1 + f_2(|\psi|) I_2\right), \tag{2.17}$$

with the invariants I_r from Equation (2.11) and the functions f_1, f_2 from Equation (2.16).

Let us note that Figure 3 on the right shows a somewhat irregular behavior of $a_1(\psi)/a_0(\psi)$ for small values $0 \leq |\psi| \leq 3$. We have thus looked at this feature in more detail by computing the numerical Ricci-flat metric for $\psi = 0.1\,n$, with $n = 0, \ldots, 30$ and fitting the results, as before, to the $k = 3$ Ansatz (2.12). The results for $a_1(\psi)/a_0(\psi)$ and $a_2(\psi)/a_0(\psi)$ in this small-$|\psi|$ range are shown in Figure 4, which indicate that $a_1(\psi)/a_0(\psi)$ does behave non-trivially around $\psi = 1$. (This non-trivial feature is of course not captured by our simple fit in Equation (2.16)).

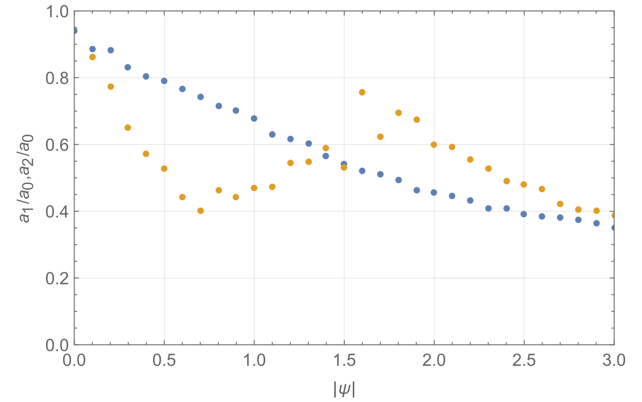

FIGURE 4 | The ratios $a_1(\psi)/a_0(\psi)$ (yellow) and $a_2(\psi)/a_0(\psi)$ (blue) for the quintic, as a function of $|\psi|$, focusing on values $\psi = 0.1\,n$, for $n = 0, \ldots, 30$, near the conifold point $\psi = 1$.

It is tempting to attribute this behavior to the conifold singularity the quintic (2.1) exhibits at $\psi = 1$. This may indeed be the case but, in view of our numerical approach, one has to be careful interpreting the effect of a singularity. For a choice of ψ near $\psi = 1$, a significant portion of the quintic's curvature is concentrated on a small locus near the (developing) conifold. As we approach $\psi = 1$, this locus becomes smaller and, at some point, can no longer be resolved in our numerical calculation, which relies on a finite point sample. In this case, the numerical metric is still a good approximate Ricci-flat metric in the "bulk" but it fails to describe the high-curvature conifold region. It is plausible that the non-trivial behavior of $a_1(\psi)/a_0(\psi)$ around $\psi = 1$ reflects this limitation of the numerical method to capture the small regions of high curvature. In summary, we expect our metric still provides an approximate Ricci-flat metric in the "bulk" but, near $\psi = 1$, it does not account for the high-curvature locus around the conifold.

3 | Approximate Ricci-Flat Metrics on the Bi-cubic

The basic strategy for bi-cubic CY manifolds follows the one for the quintic explained earlier.

3.1 | Bi-Cubic Threefolds

We start with the ambient space $\mathcal{A} = \mathbb{P}^2 \times \mathbb{P}^2$. The ambient homogeneous coordinates are denoted by x_A and y_A with $A = 0, 1, 2$, for the two $\mathbb{P}^2$ factors. On a local patch, for example the one where $x_0 \neq 0$ and $y_0 \neq 0$, we have the four affine coordinates x_a/x_0 and y_a/y_0 with $a = 1, 2$. A bi-cubic threefold X is then defined as the zero locus of a bi-degree (3,3) polynomial in $\mathcal{A}$. The non-trivial Hodge numbers are $(h^{1,1}(X), h^{2,1}(X)) = (2, 83)$, which imply the Euler number $\eta(X) = -162$. The Kähler class $[J]$ can be parametrized as $[J] = t_1[J_1] + t_2[J_2]$, where J_1 and J_2 are the restrictions of the Fubini-Study Kähler forms of the ambient $\mathbb{P}^2$ factors, and t_1, t_2 are the two Kähler parameters. In terms of these parameters, the Kähler cone is characterized by $t_1, t_2 > 0$.

There is a well-known family of bi-cubics with a freely acting symmetry defined by the cyclic generators,

$$\mathbb{Z}_3^{(1)} : \begin{cases} x_A \mapsto \alpha^A x_A \\ y_A \mapsto \alpha^A y_A \end{cases} , \qquad \mathbb{Z}_3^{(2)} : \begin{cases} x_A \mapsto x_{(A+1) \bmod 3} \\ y_A \mapsto y_{(A+1) \bmod 3} \end{cases} , \tag{3.1}$$

where $\alpha = \exp(2\pi i/3)$. If the above action is understood as a projective representation on $\mathbb{P}^2 \times \mathbb{P}^2$ the two generators commute and the total group is $\mathbb{Z}_3^{(1)} \times \mathbb{Z}_3^{(2)}$. On the other hand, understood as a linear action on $\mathbb{C}^6$ the Schur cover of $\mathbb{Z}_3^{(1)} \times \mathbb{Z}_3^{(2)}$, a group of order 27, is generated.

For our applications, we are interested in a large, non-freely acting symmetry which contains the previous one as a sub-group. This symmetry contains the two cyclic groups generated, respectively, by

$$\mathbb{Z}_3^{(x)} : \begin{cases} x_A \mapsto \alpha^A x_A \\ y_A \mapsto y_A \end{cases} , \qquad \mathbb{Z}_3^{(y)} : \begin{cases} x_A \mapsto x_A \\ y_A \mapsto \alpha^A y_A \end{cases} , \tag{3.2}$$

as well as the symmetric group, $S_3^{(x,y)}$, consisting of coordinate permutations of the form,

$$\begin{cases} x_A \mapsto x_{\sigma(A)} \\ y_A \mapsto y_{\sigma(A)} \end{cases} , \tag{3.3}$$

where $\sigma \in S_3$ is a permutation of $\{0, 1, 2\}$. Projectively, these generate a group of order 54 isomorphic to $\mathbb{Z}_3^{(x)} \times \mathbb{Z}_3^{(y)} \times S_3^{(x,y)}$, while the linear action generates a group G of order 486. The sub-space of G-invariant bi-degree (3,3) polynomials is five-dimensional and spanned by the following invariants:

$$P_1 = \sum_A x_A^3 y_A^3 , \quad P_2 = \sum_{A\neq B} x_A^3 y_B^3 , \quad P_3 = y_0 y_1 y_2 \sum_A x_A^3 ,$$
$$P_4 = x_0 x_1 x_2 \sum_A y_A^3 , \quad P_5 = x_0 x_1 x_1 y_0 y_1 y_2 \tag{3.4}$$

Within this space of G-invariants we focus on the one-parameter family of defining equations

$$P = P_1 - P_2 + 3\psi P_3 , \tag{3.5}$$

somewhat analogous to the Dwork family of quintics, where $\psi \in \mathbb{C}$ is a single complex structure parameter. This family of bi-cubics is invariant under the coordinate transformation $x_A \mapsto x_A$, $y_0 \mapsto \alpha y_0$, $y_a \mapsto y_a$, combined with $\psi \mapsto \alpha^{-1}\psi$. Therefore, the complex structure parameter should be identified as $\psi \sim \alpha\psi$. In practice, we restrict ψ to the fundamental domain $0 \leq \arg(\psi) < 2\pi/3$.

3.2 | Kähler Potential Ansatz

For the bi-cubic the simplest choice is to start with the line bundle $L = \mathcal{O}_X(1,1)$ and $k = 1$. In particular, this means we are working on the line $t_1 = t_2$ in Kähler moduli space. The space of sections $\Gamma(X, \mathcal{O}_X(1,1))$ is 9-dimensional and spanned by the monomials $x_A y_B$, where $A, B = 0, 1, 2$. There are only two G-singlets contained in $\Gamma(X, \mathcal{O}_X(1,1)) \times \Gamma(X, \mathcal{O}_X(1,1))^*$ (where G is the group generated by the actions in Equations (3.2) and (3.3)), namely

$$I_0 = \sum_{A=0}^{2} |x_A|^2 |y_A|^2 , \qquad I_1 = \sum_{A\neq B} |x_A|^2 |y_B|^2 . \tag{3.6}$$

Hence, we can write the Ansatz for the Kähler potential as

$$K = c\, t \ln(\kappa) , \qquad \kappa = a_0 I_0 + a_1 I_1 , \tag{3.7}$$

where t is the Kähler parameter along the line $t_1 = t_2$ in Kähler moduli space, that is, we take $t_1 = t_2 = t$.

3.3 | Numerical Results

We are considering the one-parameter family of bi-cubic threefolds defined by the zero locus of the polynomial P in Equation (3.5). In line with our Ansatz for the Kähler potential, we focus on Kähler parameters $t_1 = t_2 = 1$ (with the single parameter t along the line $t_1 = t_2$ easily re-instated). For the complex structure parameter ψ, we consider values of the form $\psi = 0.4n \exp(2\pi i m/18)$, where $n = 0, \ldots, 50$ and $m = 0, \ldots, 5$, covering the fundamentail domain $0 \leq \arg(\psi) < 2\pi/3$ in the range $0 \leq |\psi| \leq 20$, for a total of 301 values. As before, we have used the cymetric point generator to obtain 100000 points p_i on the manifold, for each ψ-value.

With each of these data sets we have trained a cymetric ϕ-model (width 64, depth 3, GeLU activation) for 100 epochs. The final Monge–Ampere loss as a function of ψ is shown in Figure 5, which indicates that Ricci-flat Kähler metrics have been found to a good approximation.

Furthermore, as can be seen from Figure 6 on the left, the error is relatively small, about a few percent, for small ψ but grows with $|\psi|$ to around 10%. This increase correlates with an increase in final training loss for larger $|\psi|$ and is therefore related to the residual error in the trained neural networks. It is typical that training becomes more difficult for more extreme parameter choices. While the situation can in principle be improved by taking more point samples and/or performing more extensive training, we will not attempt to improve on this as the present results are sufficient for our purposes.

The best-fit values for the coefficients a_0, a_1, and c in the ansatz (3.7) as a function of $|\psi|$ are shown in Figure 6 on

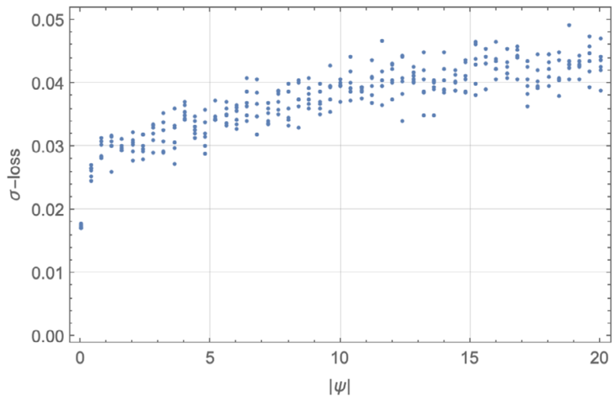

FIGURE 5 | Final σ-loss as a function of $|\psi|$ for the bicubic.

the right. Evidently, the value of c is ψ-independent to a good approximation and its mean value is $c \simeq 1/\pi$, as expected. As in our analysis of the quintic, the scatter in the data points for a_0 and a_1 in Figure 6 on the right can be reduced by removing the ambiguity due to Kähler transformations and by plotting a_1/a_0 instead. This has been done in Figure 7. As in the quintic case the result strongly suggests that a_1/a_0 is a function of only the modulus $|\psi|$. It turns out that its functional behavior can be well described by a sum of two exponentials,

$$f(|\psi|) = \frac{a_1}{a_0} \simeq 1 + 0.675 e^{-2.959|\psi|} - 0.238 e^{-0.122|\psi|}, \tag{3.8}$$

and the graph of this function is shown in Figure 7 (red curve). Hence, the expression for the Kähler potential can be written as

$$K = \frac{t}{\pi} \ln (I_0 + f(|\psi|) I_1) \tag{3.9}$$

with the invariants I_0, I_1 from Equation (3.6) and the function f from Equation (3.8).

Note that the blue points in Figure 7 indicate the asymptotic behavior $a_1/a_0 \to 1$ for $|\psi| \to \infty$. The functional form of f in Equation (3.8) has thus been chosen to reflect this feature. Assuming this is indeed the correct asymptotic form, the Kähler potential for large $|\psi|$ becomes

$$\begin{aligned} K &\simeq \frac{t}{\pi} \ln (I_0 + I_1) \\ &= \frac{t}{\pi} \ln \left(|x_0|^2 + |x_1|^2 + |x_2|^2\right) + \frac{t}{\pi} \ln \left(|y_0|^2 + |y_1|^2 + |y_2|^2\right), \end{aligned} \tag{3.10}$$

that is, a sum of the Fubini-Study Kähler potentials of the two $\mathbb{P}^2$ ambient space factors.[4]

4 | Conclusion

In this paper, we have found analytic Kähler potentials for approximately Ricci-flat metrics on certain simple Calabi–Yau (CY) manifolds. Specifically, we have considered the one-parameter family of Dwork quintic CY hyper-surfaces in $\mathbb{P}^4$ and an analogous one-parameter family of bi-cubic CY hyper-surfaces in $\mathbb{P}^2 \times \mathbb{P}^2$.

Our method is conceptually simple. Using previous result [14, 16] and the cymetric package, we have first calculated the (approximate) Ricci-flat Kähler potential numerically via machine learning methods for a number of values of the single complex structure parameter ψ. These numerical results have then been compared with Donaldson's ansatz for the Kähler potential for relatively low-degree underlying line bundles. Given the large symmetry groups of our manifolds, only a few free parameters remain in this ansatz. For each value of ψ, we have determined these parameters by a fit to the numerical data, thereby finding the "optimal" Kähler potential within the ansatz (rather than the balanced one computed by Donaldson's algorithm). The quality of the fits is quite convincing, typically reproducing the data within a few percent. This indicates that the Kähler potentials obtained provide a good approximation to the Ricci-flat ones. Moreover, after dealing with a subtlety related to Kähler transformations, we have been able to extract the explicit[5] ψ-dependence of these Kähler potentials. Perhaps somewhat unexpectedly, they only depend on the modulus, $|\psi|$, and appear to be independent of the phase of ψ, within the accuracy of our computation.

Since our motivation is to provide an analytic approximation to the Ricci-flat metric, rather than the balanced one, we have not considered performing a comparison. It is clear that the optimal metric for a given k is, by definition, closest to Ricci-flat for the given ansatz and hence, superiority to the balanced one follows, provided that the numerical metric is flat enough. Given the relatively small errors at percent level we thus expect that our approximate analytic result shares this property and is, indeed, closer to the Ricci-flat case than the balanced metric. More specifically, for the quintic the σ-loss of the numerical metric and the error of our approximation, as depicted by Figure 1, lead to the combined loss of a few percent. In particular, for the Fermat quintic with $\psi = 0$ the loss is only at percent level, indicating superiority to the balanced metric for which the σ-loss is a few tens percent [4]. It is beyond the scope of this paper to perform a systematic comparison of the two methods and we leave this to future work.

Earlier, we have presented an argument that the Ricci-flat Kähler potential has to respect the discrete symmetry G of the underlying CY manifold. We have not built this symmetry into our network architecture explicitly but, rather, have used it as a useful check of our results. The fact that the Kähler potential, numerically learned without imposing the symmetry G, fits well to the G-invariant ansatz confirms that the numerical results are sensible.[6]

The analysis of the quintic is based on the line bundle $L = \mathcal{O}_X(1)$ and we have discussed the cases of L^k, with $k = 1, 2, 3$. For $k = 1$, the optimal Kähler potential is simply the Fubini-Study Kähler potential on $\mathbb{P}^4$, restricted to the quintic. The results for the approximately Ricci-flat Kähler potentials for $k = 2, 3$ are given in Equations (2.15) and (2.17), respectively. For the one-parameter family of bi-cubics, we have considered the line bundle $L = \mathcal{O}_X(1, 1)$ for $k = 1$ and the approximately Ricci-flat Kähler potential is given in Equation (3.9).

While we have been able to determine the Kähler potential's dependence on the complex structure parameter ψ explicitly, matters are not quite so straightforward for the Kähler param-

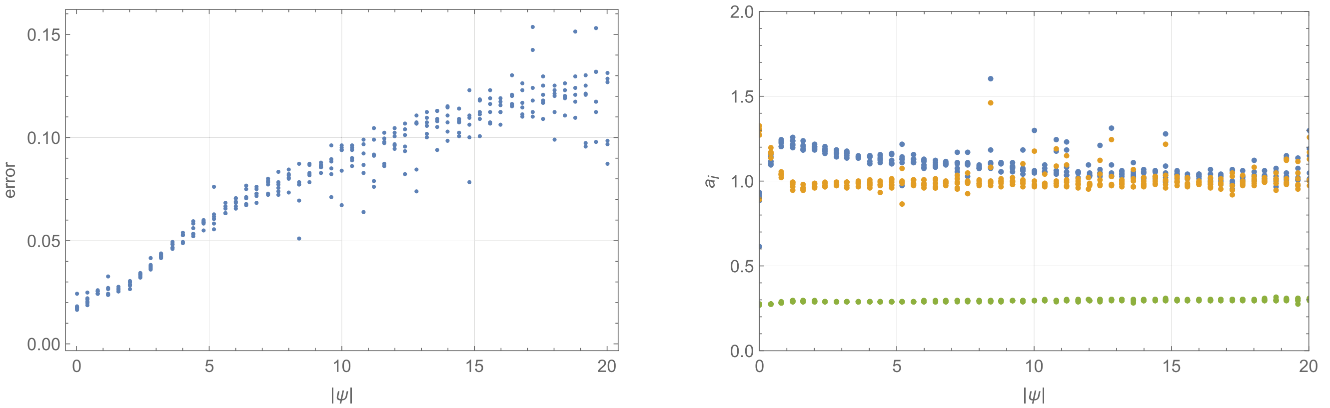

FIGURE 6 | Left plot: Mean of the relative deviation $|(K_i - K(p_i))/K(p_i)|$ as a function of ψ for the best fit of the data (p_i, K_i) to the bi-cubic Kahler potential ansatz (3.7). Right plot: Best fit values of a_0 (blue), a_1 (yellow), and c (green) in the ansatz (3.7).

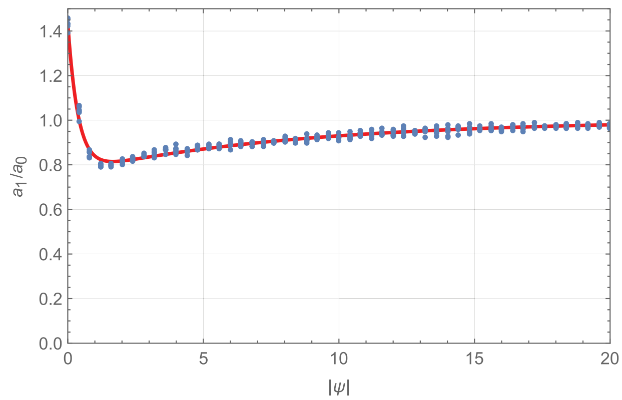

FIGURE 7 | Ratio a_1/a_0 of the best-fit parameters in the Ansatz (3.7) for the bi-cubic Kähler potential, as a function of $|\psi|$ (blue points). The red curve is a graph of the function f in Equation (3.8), the best fit of a sum of two exponentials to the data.

eters. For manifolds with a single Kähler parameter t, such as the quintic CY, the Kähler potential (and the associated metric) scales with this parameter. Therefore, in such cases, the Kähler class dependence can easily be incorporated, as has been done in Equations (2.15) and (2.17). On the other hand for CY manifolds X with $h^{1,1}(X) > 1$, such as the bi-cubic CY with $h^{1,1}(X) = 2$, the situation is more complicated. Donaldson's ansatz based on sections of a line bundle $L \to X$ is appropriate for a Kähler class $[J]$ proportional to $c_1(L)$. A change in Kähler class requires a different line bundle and leads to a completely different ansatz for the Kähler potential. It is, therefore, difficult to see how Kähler moduli dependence for cases with $h^{1,1}(X) > 1$ can be incorporated in this approach. For our example based on the bi-cubic CY, we have bypassed this difficulty by focusing on the line with $t_1 = t_2$ in Kähler moduli space.

The Kähler potentials in Equations (2.15), (2.17), and (3.9) are rather simple when expressed in terms of the projective ambient space coordinates. However, if we want to calculate the associated Kähler metric, we have to remember to restrict first to a patch in the ambient space and then to the CY hypersurface, using the defining equation. This complicates matters considerably. It remains to be seen, and is the subject of ongoing work, if our results for approximate Ricci-flat Kähler potentials can facilitate approximate analytic calculation of metric-dependent quantities, despite these difficulties.

Acknowledgements

S.J.L. thanks the University of Oxford, where part of this work was completed, for hospitality. The work of S.J.L. was supported in part by the Yonsei University Research Fund 2025-22-0134. A.L. thanks the Institute for Basic Science (IBS) in Daejeon, where part of this work was done, for hospitality. A.L. is supported in part by the STFC grant ST/X000761/1.

Conflicts of Interest

The authors declare no conflicts of interest.

Data Availability Statement

The data that support the findings of this study are available upon reasonable request.

Endnotes

[1] See also [19] for a related analysis of highly symmetric CY manifolds such as the Fermat quintic, for which approximately Ricci-flat analytic metrics are sought after in terms of symmetric polynomials.

[2] This also works for general quintics since the matrix H in Equation (2.5) can be diagonalized to a unit matrix using a suitable GL(5) transformation acting on the homogeneous coordinates.

[3] Strictly speaking, any values of the complex structure ψ with $m = 5$ do not lie in the fundamental domain and should rather be considered redundant, as they are identified with their $m = 0$ counterparts. Nevertheless, we still include them in our analysis for a sanity check.

[4] The parametrization (3.5) indicates that the hypersurface degenerates in the large ψ limit into the union of the four irreducible components, $E \times \mathbb{P}^2$ and $\mathbb{P}^2 \times H_A$ with $A = 0, 1, 2$, where E is the Fermat-type elliptic curve in the first $\mathbb{P}^2$ ambient factor and $H_A = \{y_A = 0\} \subset \mathbb{P}^2$ are the hyperplanes in the second. Given this asymmetric form of the variety, it is not clear to us if there is a fundamental reason behind the factorization of the metric.

[5] Note that the ψ-dependence of the Kähler potential has directly been learned in [12], for the Dwork family of the quintic.

[6] See Ref. [22] for an invariant machine learning approach, where the symmetry is reflected in the neural network architecture.

References

1. S. K. Donaldson, "Some Numerical Results in Complex Differential Geometry," preprint, arXiv, December 28, 2005.

2. M. R. Douglas, R. L. Karp, S. Lukic, and R. Reinbacher, "Numerical Solution to the Hermitian Yang-Mills Equation on the Fermat Quintic," *Journal of High Energy Physics* 12 (2007): 083, [arXiv:hep-th/0606261 [hep-th]].

3. M. R. Douglas, R. L. Karp, S. Lukic, and R. Reinbacher, "Numerical Calabi-Yau Metrics," *Journal of Mathematical Physics* 49 (2008): 032302, [arXiv:hep-th/0612075 [hep-th]].

4. V. Braun, T. Brelidze, M. R. Douglas, and B. A. Ovrut, "Calabi-Yau Metrics for Quotients and Complete Intersections," *Journal of High Energy Physics* 05 (2008): 080, [arXiv:0712.3563 [hep-th]].

5. V. Braun, T. Brelidze, M. R. Douglas, and B. A. Ovrut, "Eigenvalues and Eigenfunctions of the Scalar Laplace Operator on Calabi-Yau Manifolds," *Journal of High Energy Physics* 07 (2008): 120, [arXiv:0805.3689 [hep-th]].

6. L. B. Anderson, V. Braun, R. L. Karp, and B. A. Ovrut, "Numerical Hermitian Yang-Mills Connections and Vector Bundle Stability in Heterotic Theories," *Journal of High Energy Physics* 06 (2010): 107, [arXiv:1004.4399 [hep-th]].

7. L. B. Anderson, V. Braun, and B. A. Ovrut, "Numerical Hermitian Yang-Mills Connections and Kahler Cone Substructure," *Journal of High Energy Physics* 01 (2012): 014, [arXiv:1103.3041 [hep-th]].

8. M. Headrick and A. Nassar, "Energy Functionals for Calabi-Yau Metrics," *Advances in Theoretical and Mathematical Physics* 17, no. 5 (2013): 867–902, [arXiv:0908.2635 [hep-th]].

9. W. Cui and J. Gray, "Numerical Metrics, Curvature Expansions and Calabi-Yau Manifolds," *Journal of High Energy Physics* 05 (2020): 044, [arXiv:1912.11068 [hep-th]].

10. A. Ashmore, Y. H. He, and B. A. Ovrut, "Machine Learning Calabi–Yau Metrics," *Fortschritte der Physik* 68, no. 9 (2020): 2000068, [arXiv:1910.08605 [hep-th]].

11. M. R. Douglas, S. Lakshminarasimhan, and Y. Qi, "Numerical Calabi-Yau Metrics From Holomorphic Networks," preprint, arXiv, December 9, 2020, [arXiv:2012.04797 [hep-th]].

12. L. B. Anderson, M. Gerdes, J. Gray, S. Krippendorf, N. Raghuram, and F. Ruehle, "Moduli-Dependent Calabi-Yau and SU(3)-Structure Metrics From Machine Learning," *Journal of High Energy Physics* 05 (2021): 013, [arXiv:2012.04656 [hep-th]].

13. V. Jejjala, D. K. Mayorga Pena, and C. Mishra, "Neural Network Approximations for Calabi-Yau Metrics," *Journal of High Energy Physics* 08 (2022): 105, [arXiv:2012.15821 [hep-th]].

14. M. Larfors, A. Lukas, F. Ruehle, and R. Schneider, "Learning Size and Shape of Calabi-Yau Spaces," preprint, arXiv, November 02, 2021, [arXiv:2111.01436 [hep-th]].

15. A. Ashmore, L. Calmon, Y. H. He, and B. A. Ovrut, "Calabi-Yau Metrics, Energy Functionals and Machine-Learning," *International Journal of Data Science in the Mathematical Sciences* 1, no. 1 (2023): 49–61, [arXiv:2112.10872 [hep-th]].

16. M. Larfors, A. Lukas, F. Ruehle, and R. Schneider, "Numerical Metrics for Complete Intersection and Kreuzer–Skarke Calabi–Yau Manifolds," *Machine Learning: Science and Technology* 3, no. 3 (2022): 035014, [arXiv:2205.13408 [hep-th]].

17. F. Ruehle and B. Sung, "Attractors, Geodesics, and the Geometry of Moduli Spaces," preprint, arXiv, August 1, 2024, [arXiv:2408.00830 [hep-th]].

18. A. Constantin, C. S. Fraser-Taliente, T. R. Harvey, A. Lukas, and B. Ovrut, "Computation of Quark Masses From String Theory," *Nuclear Physics B* 1010 (2025): 116778, [arXiv:2402.01615 [hep-th]].

19. V. Mirjanić and C. Mishra, "Symbolic Approximations to Ricci-Flat Metrics Via Extrinsic Symmetries of Calabi–Yau Hypersurfaces," *Machine Learning: Science and Technology* 6, no. 3 (2025): 035029, [arXiv:2412.19778 [hep-th]].

20. T. Hubsch, *Calabi-Yau Manifolds: A Bestiary for Physicists* (World Scientific Singapore, 1994).

21. D. Joyce, *Compact Manifolds with Special Holonomy* (OUP, 2000).

22. Y. Hendi, M. Larfors, and M. Walden, "Learning Group Invariant Calabi-Yau Metrics by Fundamental Domain Projections," *Machine Learning: Science and Technology* 6, no. 1 (2025): 015050, [arXiv:2407.06914 [hep-th]].